2018 European Control Conference (ECC)
June 12-15, 2018. Limassol, Cyprus

Modeling and power management of a LEO small satellite electrical power system

Elisa Mostacciuolo[♮], Luigi Iannelli[♮], Salvatore Sagnelli[†], Francesco Vasca[♮], Raffaele Luisi[†], Vincenzo Stanzione[†]

Abstract— **The main task of the electrical power system (EPS) of a low earth orbit (LEO) satellite consists of providing the required power to the payloads by regulating, controlling and distributing the power generated by the solar array and the battery. The choice of an efficient EPS configuration and the design of an effective power management strategy are crucial elements for the success of the mission and the satellite lifetime. In this paper a dynamic model for a peak power tracker EPS architecture with an unregulated bus for small satellites is proposed. The model is used to verify the solar array and the battery sizing under different operating conditions. A power management strategy based on a finite-state supervisor is proposed and its effectiveness is verified through the EPS model by considering different irradiance and temperature profiles.**

I. Introduction

The combination of commercial-off-the-shelf microelectronic technologies developed for terrestrial use and adapted to the space environment and the increasing capabilities of low-power microelectronics, has encouraged the development of a new class of highly capable smaller, faster, cheaper satellites complementing the conventional large satellite systems [1], [2]. As a result, it is observed an increasing interest in small and micro satellites design and, more specifically, in the use of simulation analysis for the deployment the control of the satellite subsystems [3]–[6]. The electrical power system (EPS) plays a crucial role in the lifetime of small satellites. Indeed, the EPS should be effectively compliant to several requirements in order to provide power generation, management, storage, control, protection and distribution to the spacecraft payloads and platform equipments during the entire mission life. From the regulation point of view the EPS shall manage peak, pulse and transient power demands and the battery charge/discharge cycle by avoiding spacecraft instability and performance degradation.

At a certain level of abstraction, a quite general architecture of an EPS can be decomposed into four main blocks: a primary power source, an energy storage, a power management unit that deals with power conditioning and charge/discharge control, and a power distribution unit [7], [8]. The sizing of the subsystems and the design of an efficient power management strategy are complex and critical tasks usually undertaken in the satellite design phase [9], [10]. A conceptual design of a spacecraft power system involves an optimal selection of available technologies of different components, such as solar cells, solar arrays, batteries, and bus voltages. However the electrical architecture of spacecrafts is not standard and shall, in general, need to be adapted nearly case by case. Thus, the identification of the topology is the preliminary step for the EPS design. There are several basic topologies, that can be classified based on two main criteria: the energy transfer and the voltage main bus regulation [11], [12].

The primary satellite power can be fed to the main power bus according to two different conditioning topologies: a direct energy transfer or a peak power tracker (PPT). In the former approach the solar power is delivered to the loads (and equipments) with no series regulation unit; the excess power is typically shunt to ground trough parallel switches [13]. In the PPT topology the regulated power is provided to the main bus by DC-DC power converters [14]. The converters are controlled as a function of the required bus power demand by extracting the appropriate operating point on the solar array (SA) power characteristic up to the maximum power.

In this paper we refer to a maximum power point tracker (MPPT) topology with unregulated bus for a low earth orbit (LEO) small satellite. Nowadays the PPT topology is a promising solution for miniature satellites because of the use of higher efficient solar cell, better MPPT techniques and low cost/low mass MPPT modules. Furthermore the PPT is well-suited to LEO orbits due to the wide range of variation in sun projection over the solar array. We propose a modular dynamic model for the EPS and a corresponding power management policy. The model and the power splitting strategy are verified through numerical simulations of the satellite behavior under several environmental and load conditions. The model is shown to be also useful for the verification of the solar array and the storage sizing.

The rest of the paper is organized as follows. In Section II the architecture under study is presented, while in Section III the models of all EPS subsystems are described. Section IV deals with the proposed power split policy. The effectiveness of our model and control strategy is confirmed by the simulation results discussed in Section V. Finally, in Section VI the research conclusions are summarized.

[♮] Department of Engineering, University of Sannio, 82100 Benevento, Italy, email: elisa.mostacciuolo@unisannio.it, luigi.iannelli@unisannio.it, vasca@unisannio.it.

[†]SITAEL S.p.A., 70042 Mola di Bari, Bari, Italy, email: salvatore.sagnelli@sitael.com, vincenzo.stanzione@sitael.com , raffaele.luisi@sitael.com. The research activity has been developed within a collaboration between the Department of Engineering of the University of Sannio and SITAEL S.p.A.

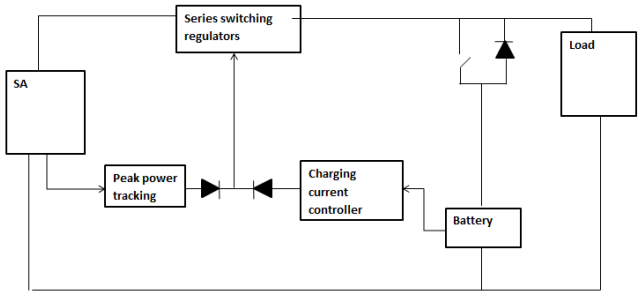

Fig. 1. The considered PPT with unregulated bus architecture.

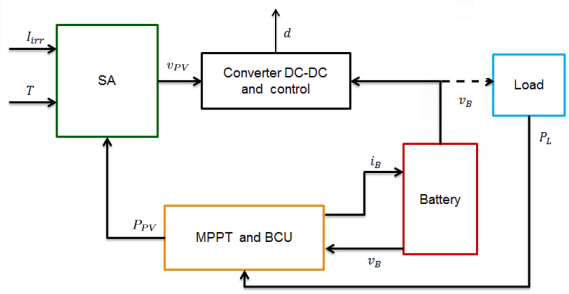

Fig. 2. A block scheme of the EPS model.

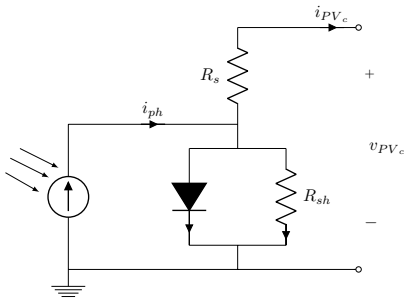

Fig. 3. An equivalent circuit for a solar cell.

II. EPS ARCHITECTURE

The PPT topology analyzed in this paper considers an individual MPPT module for each photovoltaic panel, thus allowing the use of different cell technology and string length for each panel and improving the system reliability. Furthermore, the peak power point of each panel is tracked individually, which allows an efficiency improvement. Indeed, the panels of spin stabilized LEO satellites can operate under different irradiance and temperature conditions.

The PPT topologies are characterized by the different power conditioning bus architecture: regulated [10], [15], [16] or unregulated [17]. We consider a PPT topology with an unregulated bus, see Fig. 1. The main bus voltage is provided by the battery output voltage which is upper and lower bounded and it increases during charge phases and decreases during the discharge ones.

The unregulated bus allows EPS mass and cost savings. It is particularly advantageous in case of power bus operations with short but high peak loads or with impulsive power profiles occurring during radar instrument operations. Moreover it allows higher numerical and functional EPS reliability because of reduced electronic circuitry [18]. The MPPT with unregulated bus offers about 9% SA surface reduction (compared with direct energy transfer solutions) but imposes some constraints on thermal interfaces, indeed dissipation inside the power and control distribution unit is higher. It also introduces additional constraints on the MPPT —as this now needs to ensure the correct charging strategy for the battery, independent of bus load— a function normally carried out by a separate battery charge regulator.

III. EPS MODEL

The proposed modular EPS model is based on a power flow representation. An equivalent scheme of the model is reported in Fig. 2. The environment acts on the considered system through some input signals which depend on the satellite mission: the solar irradiance I_{rr} and the temperature T, which vary along the orbit and the loads' power consumptions. The irradiance and the temperature are inputs for the SA block which provides, based on the power request coming from the MPPT, the SA voltage v_{PV}. For the sake of readability we assume one PV panel and one DC-DC converter, i.e. the SA output voltage v_{PV} corresponds to the PV panel output voltage. The battery model consists of two dynamic equations coupled with state of charge (SOC) maps.

The control block includes the MPPT strategy and the battery control unit (BCU). This subsystem, by using as inputs the load power P_L and the battery voltage v_B, determines the power requested from the SA and the battery current. The SA and battery voltages allow the computation of the duty cycle for the modulation of the DC-DC converter in order to satisfy the power request.

All constants and parameters of the model are determined based on solar cell and battery datasheet. The model is implemented in the Matlab-Simulink platform, and its subsystems are detailed in the following subsections.

A. Solar array model

The SA consists of several PV panels, each modeled with a certain number of PV cells connected in a series−parallel combination such that the required voltage and current are obtained.

A typical steady state equivalent electrical circuit for a solar cell is shown in Fig. 3. The cell acts as a current source shunted by an ideal diode. The series resistor R_s represents the internal resistance to the current flow, due to the resistivity of the material. The shunt resistor R_{sh} determines the leakage current across the junction and its value is related to the junction depth, the impurities and the contact resistance. In an ideal PV cell, there are no series losses and no leakage to ground, i.e. R_s is a short circuit and R_{sh} is an open circuit.

The electrical model can be derived by considering an ideal diode characteristic, n_s cells in series and n_p cells in parallel. The current provided by each PV panel is the sum

of the n_p currents obtained by the cells in parallel and it can be written as

$$i_{PV} = f(i_{PV}, v_{PV}) \tag{1}$$

with

$$\begin{aligned} f(i_{PV}, v_{PV}) =& n_p i_{ph}(T, I_{rr}) \\ & - I_0(T) n_p \Big[e^{\left(\frac{q}{nKT}\left(\frac{v_{PV}}{n_s} + \frac{R_s i_{PV}}{n_p}\right)\right)} - 1 \Big] \\ & - \frac{n_p v_{PV} + n_s i_{PV} R_s}{n_s R_{sh}} \end{aligned} \tag{2}$$

where $v_{PV} = n_s v_{PV_c}$ is the total PV panel output voltage obtained as the sum of the voltages provided by the series-connected cells, K is the Boltzmann constant, n is the diode ideality factor, q is the electron charge, I_0 is the diode saturation current, T is the temperature on the photovoltaic panel which is considered as an input together with the irradiance I_{rr} and $i_{ph}(T, I_{rr})$ is the photo-generated current.

By writing the PV current in terms of its voltage and power and by substituting $i_{PV} = P_{PV}/v_{PV}$ in (1) one can write

$$P_{PV} = v_{PV} f(P_{PV}/v_{PV}, v_{PV}). \tag{3}$$

Given the desired power P_{PV}, the temperature T, the irradiance I_{rr}, the maps of the photo-generated current $i_{ph}(T, I_{rr})$ and the map of the saturation current $I_0(T)$, one can numerically solve (3) with (2) in order to obtain the PV voltage v_{PV}.

B. Solar array maps and parameters

The maps for the photo-generated current $i_{ph}(T, I_{rr})$ and that for the diode saturation current $I_0(T)$ are evaluated by considering (1) under specific operating conditions. By assuming the open circuit voltage $v_{PV} = V_{oc}(T)$ and current $i_{PV} = 0$, from (1) one obtains

$$i_{ph}(T, I_{rr}) = I_0(T) \Big[e^{\left(\frac{qV_{oc}(T)}{nKTn_s}\right)} - 1 \Big] + \frac{V_{oc}(T)}{n_s R_{sh}}. \tag{4}$$

Moreover, by imposing the short circuit conditions $v_{PV} = 0$ and $i_{PV} = I_{sc}$, the expression (1) becomes

$$\begin{aligned} I_{sc}(T) =& n_p i_{ph}(T, I_{rr}) - I_0(T) n_p \Big[e^{\left(\frac{qR_s I_{sc}(T)}{nKTn_p}\right)} - 1 \Big] \\ & - \frac{I_{sc}(T) R_s}{R_{sh}}. \end{aligned} \tag{5}$$

The short circuit current I_{sc} and the open circuit voltage V_{oc} can be usually approximated as affinely dependent on the temperature:

$$I_{sc}(T) = I^*_{sc}(1 + K_i(T - T^*)) \tag{6a}$$

$$V_{oc}(T) = V^*_{oc}(1 + K_v(T - T^*)) \tag{6b}$$

with V^*_{oc} and I^*_{sc} standard test condition values, i.e. with temperature T^* and irradiance I^*_{rr}, and K_i and K_v the temperature coefficients of short circuit current and open circuit voltage, respectively, [19]. By using (6) in (4) and (5) one can easily obtain the maps of the photo-generated and saturation currents as a function of the temperature and irradiance.

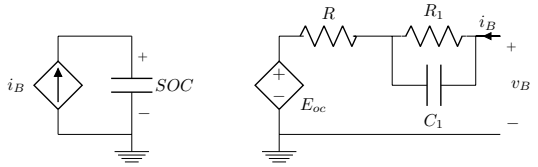

Fig. 4. Equivalent electrical circuit or the battery model.

The SA model requires also to fix the diode ideality factor n, the series resistance R_s and the shunt resistance R_{sh}. These constants can be obtained from the maximum power point values, which can be represented through the following relations [20]

$$I^*_{MPP} = f(I^*_{MPP}, V^*_{MPP}), \tag{7a}$$

$$\left.\frac{\partial i_{PV}}{\partial v_{PV}}\right|_{\substack{v_{PV}=0 \\ i_{PV}=I_{sc}}} = -\frac{1}{R_{sh}}, \tag{7b}$$

$$\left.\frac{\partial P_{PV}}{\partial v_{PV}}\right|_{\substack{v_{PV}=V^*_{MPP} \\ i_{PV}=I^*_{MPP}}} = 0, \tag{7c}$$

with the function $f(\cdot)$ defined by (2), V^*_{MPP} and I^*_{MPP} the voltage and the current at the maximum power point in standard test condition, respectively, provided by the datasheet and I_{sc} given by (6a). From (7c) one obtains

$$\left.\left(i_{PV} + v_{PV}\frac{\partial i_{PV}}{\partial v_{PV}}\right)\right|_{\substack{v_{PV}=V^*_{MPP} \\ i_{PV}=I^*_{MPP}}} = 0 \tag{8}$$

where the expression of the partial derivative of the current with respect to the voltage can be obtained from (1) by using the implicit function derivative theorem which provides

$$\frac{\partial i_{PV}}{\partial v_{PV}} = \frac{\frac{\partial f(i_{PV}, v_{PV})}{\partial v_{PV}}}{1 - \frac{\partial f(i_{PV}, v_{PV})}{\partial i_{PV}}} \tag{9}$$

where $f(\cdot)$ is given by (2).

C. Battery model

The battery model is obtained by considering the equivalent electrical circuit shown in Fig. 4, see [21]. The model considers as input the current i_B and as state variables the internal battery voltage v_1 and the state of charge SOC. Since also the thermal effects want to be considered, a further state variable is the battery temperature T_B.

By applying the Kirchhoff current law, the dynamic equation for the internal voltage can be written as

$$C_1 \frac{\mathrm{d}}{\mathrm{d}t} v_{C_1} = -\frac{1}{R_1} v_{C_1} - i_B \tag{10}$$

where R_1 and C_1 are the internal resistance and capacitor, respectively.

The battery voltage, which is an output for the battery subsystem, can be evaluated as a function of the open circuit voltage E_{oc}, the current i_B and the internal voltage v_1. By applying the Kirchhoff voltage law to the circuit in Fig. 4,

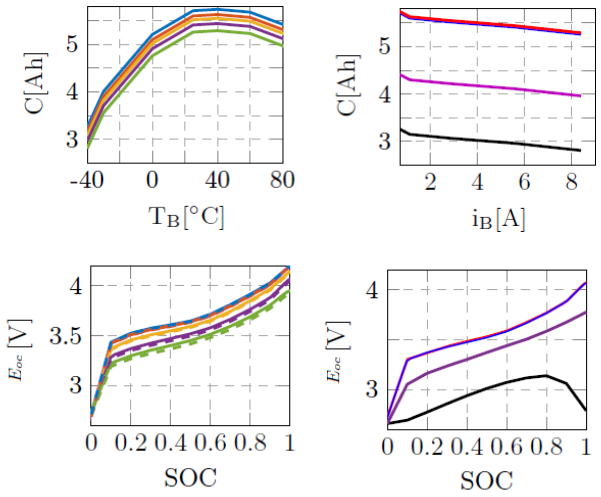

Fig. 5. The maps adopted for the battery model: C vs T_B for different values of the current (top left), C vs i_B for different values of the temperature (top right), E_{oc} vs SOC for different values of the current (bottom left) and temperature (bottom right). The black, violet, blue, and red lines, correspond to -40 °C, -20 °C, 25 °C, and 40 °C, respectively. The blue, red, yellow, violet and green lines correspond to 0.7 A, 1.12 A, 2.8 A, 5.6 A, 8.4 A while the dashed lines are the current characteristics during the discharging phase.

one can write

$$v_B = E_{oc}(SOC, i_B, T_B) + Ri_B - v_{C_1}, \tag{11}$$

where R is the series resistance and E_{oc} is a nonlinear function of the state of charge SOC, battery current i_B and battery temperature T_B. The SOC is obtained by integrating the battery current

$$\frac{\mathrm{d}}{\mathrm{d}t}SOC = \frac{1}{C(T_B, i_B)} i_B, \tag{12}$$

where C is the battery capacity which depends on the current (discharge rate effect) and on the battery internal temperature T_B. The map that provides the value of the battery capacity C for given values of current i_B and temperature T_B is shown in Fig 5. For high values of the current we have low capacity, i.e. the cut-off voltage corresponds to a value of the capacity lower than the one corresponding to a higher current. The relation between E_{oc} and SOC changes under varying conditions, i.e. the charge/discharge current and the temperature [22]. We model these dependencies through a map deduced from the cell datasheet, see Fig. 5. Note that during the discharge phase, E_{oc} is lower than the one corresponding to the charge phase for the same SOC.

The electrical variables of the battery are also influenced by the temperature. The thermal model allows the computation of the battery temperature time evolution by considering as inputs the ambient-temperature T_a and the power dissipated due to the Joule effect P_{diss} [23]. By considering a thermal dynamic equation one can write

$$C_{th}\frac{\mathrm{d}}{\mathrm{d}t}T_B = -\frac{1}{R_{th}}(T_B - T_a) + P_{diss}(v_{C_1}, i_B) \tag{13}$$

where the dissipated power is given by

$$P_{diss}(v_{C_1}, i_B) = \frac{v_{C_1}^2}{R_1} + Ri_B^2 \tag{14}$$

and R_{th} and C_{th} are the thermal resistance and the thermal capacity, respectively.

IV. Control Strategy

The power dispatch is a critical issue in a satellite mission; a power system failure means the loss of a mission. The power control strategy needs to satisfy the power demand according to the available maximum power and to determine the power that the SA has to provide together with the charge or discharge battery current.

A. Maximum power points computation

To implement an efficient control strategy it is necessary to compute the panel voltage V_{MPP} and the panel current I_{MPP} at the maximum power point, according to the measured temperature and irradiance. The variations of V_{MPP} and I_{MPP} with respect to their nominal values V^*_{MPP} and I^*_{MPP} can be assumed to have a linear dependence with respect to the temperature variation and a logarithmic dependence with respect to the irradiance ratio [24]. Therefore, the voltage and the current at MPP can be expressed as

$$V_{MPP} = \begin{cases} V^*_{MPP} + \frac{q}{nKT^*}\ln\left(\frac{I_{rr}}{100}\right)\ln\left(\frac{I_{rr}}{I^*_{rr}}\right) + \delta_V(T - T^*) \\ \qquad\qquad \text{if } I_{rr} \geq 100\frac{W}{m^2}, \\ V^*_{MPP} + \frac{q}{nKT^*}\ln\left(\frac{I_{rr}}{100}\right) + \delta_V(T - T^*) \\ \qquad\qquad \text{if } I_{rr} < 100\frac{W}{m^2}. \end{cases} \tag{15a}$$

$$I_{MPP} = I^*_{MPP}\left(\frac{I_{rr}}{I^*_{rr}}\right)(1 + \delta_I(T - T^*)) \tag{15b}$$

where δ_V and δ_I are the voltage and current temperature coefficients, respectively, and I^*_{rr} is the irradiance in standard test condition.

B. Battery charging process

A widely diffused strategy for the battery charging is the so-called constant current-constant voltage (CC/CV) algorithm which is also considered herein. The algorithm consists of three phases, see Fig. 6: the preCharge mode, the CC mode that ends when the battery reaches the maximum value of the voltage and the CV mode where the voltage is constant while the current has an exponential decay.

We define a boolean variable, say γ_B, which indicates the start of the charging process. This signal is obtained by considering SOC and the beginning of the eclipse and the sunlight phases, respectively. Indeed the battery should be re-charged at the beginning of the sunlight phase and when SOC is below its minimum value. Moreover the battery has to be fully charged at the beginning of each eclipse. The duration of the charging process, say Δ_{ch}, can be obtained by integrating the SOC dynamics with the assumption of the pre-defined charging profile, see Fig. 6, where t_1, I_{B_1},

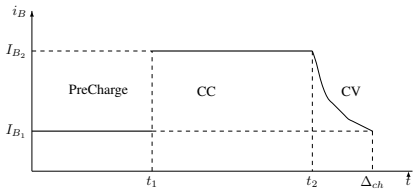

Fig. 6. A typical battery current profile for the CC-CV algorithm.

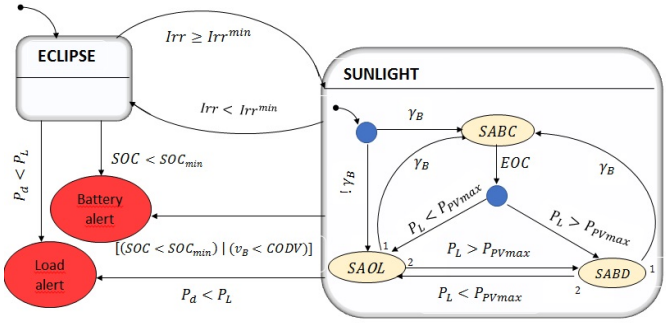

Fig. 7. Finite-state machine of the supervisor.

I_{B_2} and α_B are known. In particular, one can write

$$C_{nom}SOC(\Delta_{ch}) = C_{nom}SOC(0) + I_{B_1}t_1 + I_{B_2}(t_2 - t_1) - \frac{1}{\alpha_B}I_{B_2}(e^{-\alpha_B(\Delta_{ch}-t_2)} - 1) \quad (16a)$$

$$\Delta_{ch} = -\frac{1}{\alpha_B}\ln\left(\frac{I_{B_1}}{I_{B_2}}\right) + t_2 \quad (16b)$$

where C_{nom} is the nominal value of the battery capacity, t_1 and t_2 are the time instants at which the CC and CV phases start, I_{B_1} and I_{B_2} are the current values for the PreCharge and CC modes and α_B is the coefficient that determines the current exponential decay during the CV mode.

C. Power management control strategy

The proposed power management policy can be described through the scheme shown in Fig. 7. Given the temperature and irradiance profiles for each panel, the load demand P_L, the battery state of charge SOC and the corresponding voltage v_B, the power requested to the SA and the battery current are determined. Two alerts highlight the incomplete battery charging and/or the possible deficit power supplied to the load.

The behavior of the satellite differs if it is in sunlight or in eclipse. Indeed, during the eclipse phase, the battery is the only power source for the satellite. Then the power requested to the solar array is zero while the discharging current i_B is determined according to v_B and P_B. The value of the discharging current is limited to its maximum.

During sunlight we can distinguish three satellite operative modes corresponding to three control states: SA only loads (SAOL), SA battery discharge (SABD) and SA battery charge (SABC). The SAOL state is active if the battery has not to be recharged, i.e. the signal γ_B is low, and P_L is less than the maximum power point of the solar array. During the SAOL state, the solar array only supplies the power required by the loads. During the SABD mode the battery has not to be recharged and P_L is larger than the maximum power point of the SA. Then the power required by the loads is supplied by the SA together with the battery. Finally the SABC state is active if the battery has to be recharged, i.e. the signal γ_B is high. The SA provides the needed power to charge the battery and to the loads. The state is deactivated when the battery is fully charged. The logic of the SABC state is illustrated in Algorithm 1. If the SA cannot supply enough power to charge the battery and satisfy the load demand, the priority is given to the loads.

Algorithm 1: preCharge/CCmode/CVmode

Input: P_L, v_B, P_{XMmax}, P_{XPmax}, P_{YMmax}, P_{YPmax}, P_{PVmax}
Output: i_B, P_{XM}, P_{XP}, P_{YM}, P_{YP}, P_d
begin
/*Current evaluation*/;
$i_B \leftarrow I_B^*$;
/*where: $I_B^* \leftarrow I_{B1}$ in preCharge, $I_B^* \leftarrow I_{B2}$ in CCmode, $I_B^* \leftarrow I_{B2}e^{-\alpha_B(t-t_2)}$ in CVmode*/;
/*Battery power estimation */;
$P_B \leftarrow v_B i_B$;
/*Required power evaluation/;
$P_{PV} \leftarrow P_L + P_B$;
/*Check supplied power */;
if $(P_{PV} > P_{PVmax})$ **then**
$P_{PV} \leftarrow P_{PVmax})$;
/*Maximum power to be supplied to the battery*/;
$P_B \leftarrow P_{PV} - P_L$;
/*Current evaluation/;
$i_B \leftarrow \frac{P_B}{v_B}$;
end
/*Power available*/;
$P_d \leftarrow P_{PV} - v_B i_B$;
/*The function `setPV` determine the power requests to each panel by considering the maximum power available and the maximum power of each panel.*/;
$(P_{XM}, P_{XP}, P_{YM}, P_{YP}) \leftarrow$ `setPV`$(P_{XMmax}, P_{XPmax}, P_{YMmax}, P_{YPmax}, P_{PV})$;
end

V. Simulation Results

The effectiveness of the power management strategy is demonstrated through several numerical tests. For each panel we use typical LEO environmental conditions (e.g. temperature and irradiance). We also define a strategy to dispatch the requested power to the four panels according to the effective maximum power point.

The technical data and the parameters of the model are: a MP176065xtd battery, a CESI CTJ-30 solar cell, $n_s = 32$, $n_p = 8$, $Ta = 298$ K, $R_{th} = 7.44$ KW^{-1}, $C_{th} = 483.57$ JK^{-1}, R =11 mΩ, R_1 =15 mΩ and $C_1 = 1.5$ kF, $T^* = 25$ °C, $I_{rr}^* = 1000$ Wm^{-2}, total sunlight duration 5400 s, eclipse duration 3000 s.

The profiles of the power provided to the storage (negative if it is supplied by) and the power requested from the SA are reported in Fig. 8. The first PV panel operates at its maximum power point $P_{XM_{max}}$ while the power furnished by the SA P_{PV} is almost always below its maximum value, i.e. not all the PV panels operate at their respective maximum power points. The temperature, the current, the voltage and the SOC of the battery are reported in Fig. 9. The parameters used for the simulations are reported in the Appendix.

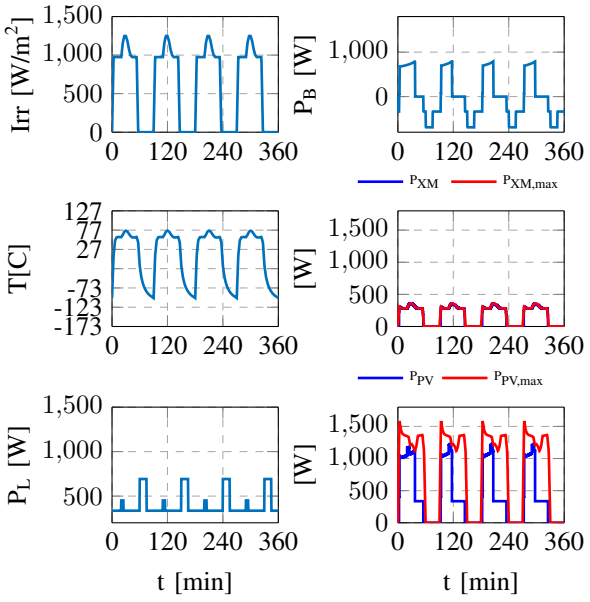

Fig. 8. The irradiance and the temperature experienced from the first PV panel (top and middle left respectively), the power load request (bottom left), the battery power (top right) and the power requested from the first panel and from the SA respectively (middle and bottom right) are reported. The red lines indicate the maximum power that can be supplied.

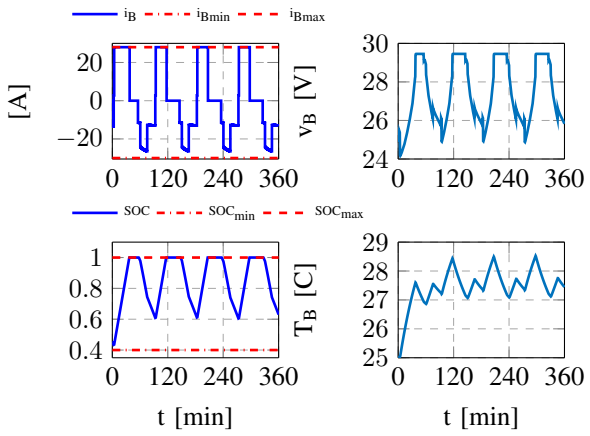

Fig. 9. Time evolutions of he current and the voltage of the battery (top left and right), the state of charge and the temperature (bottom left and right).

VI. Conclusion

The EPS design is a very critical point in small LEO satellites. We have proposed an EPS dynamic model and a strategy for the power splitting between the solar array and the battery under different operating conditions determined by sunlight and eclipse intervals, irradiance, temperatures and loads. The model is shown to be useful for the verification of the spacecraft subsystems sizing for a given mission. Simulation results have shown the effectiveness of the proposed power management strategy. Future work will analyze the use of the model for the optimization of the battery charging and discharging operations.

References

[1] P. Fortescue, G. Swinerd, and J. Stark, *Spacecraft systems engineering*. United Kingdom: John Wiley & Sons, 2011.

[2] J. Bouwmeester and J. Guo, "Survey of worldwide pico-and nanosatellite missions, distributions and subsystem technology," *Acta Astronautica*, vol. 67, no. 7, pp. 854–862, 2010.

[3] A. Ali, M. R. Mughal, H. Ali, and L. Reyneri, "Innovative power management, attitude determination and control tile for cubesat standard nanosatellites," *Acta Astronautica*, vol. 96, pp. 116–127, 2014.

[4] M. Raif, U. Walter, and J. Bouwmeester, "Dynamic system simulation of small satellite projects," *Acta Astronautica*, vol. 67, no. 9, pp. 1138–1156, 2010.

[5] M. U. Khan, A. Ali, H. Ali, M. S. Khattak, and I. Ahmad, "Designing efficient electric power supply system for micro-satellite," in *International Conference on Computing, Electronic and Electrical Engineering*, Quetta, Pakistan, Apr 2016, pp. 207–212.

[6] S. Corpino and F. Stesina, "Verification of a cubesat via hardware-in-the-loop simulation," *IEEE Transactions on Aerospace and Electronic Systems*, vol. 50, no. 4, pp. 2807–2818, 2014.

[7] J. R. W. Wiley J. Larson, *Space Mission Analysis and Design*. United States: Space Technology Library, 2005.

[8] W. H. Ley Wilfried, Klaus Wittmann, *Handbook of space technology*. United Kingdom: John Wiley & Sons, 2009.

[9] D. Del Corso, C. Passerone, L. Reyneri, C. Sansoe, S. Speretta, and M. Tranchero, "Design of a university nano-satellite: The picpot case," *IEEE Transactions on Aerospace and Electronic Systems*, vol. 47, no. 3, pp. 1985–2007, 2011.

[10] P. T. Huynh and B. H. Cho, "Design and analysis of a regulated peak-power tracking system," *IEEE Transactions on Aerospace and Electronic systems*, vol. 35, no. 1, pp. 84–92, 1999.

[11] O. Shekoofa and E. Kosari, "Comparing the topologies of satellite electrical power subsystem based on system level specifications," in *6th International Conference on Recent Advances in Space Technologies*, Istanbul, Turkey, Jun 2013, pp. 671–675.

[12] D. Erb, S. Rawashdeh, and J. Lumpp Jr, "Evaluation of solar array peak power tracking technologies for cubesats," in *25th Annual AIAA/USU Conference on Small Satellites*, Logan, Utah, Aug 2011, pp. 1–10.

[13] M. Zahran, S. Tawfik, and G. Dyakov, "LEO satellite power subsystem reliability analysis," *Journal of Power Electronics*, vol. 6, no. 2, pp. 104–113, 2006.

[14] S. Bifaretti, S. Pipolo, T. Catalano, G. Daprati, V. Iacovone, and E. Scione, "Functional study of a distributed MPPT power management system," in *11th European Space Power Conference*, Thessaloniki, Greece, Oct 2016, pp. 1–5.

[15] S.-S. Jang, S.-H. Kim, S.-R. Lee, and J. Choi, "Energy balance and power performance analysis for satellite in low earth orbit," *Journal of Astronomy and Space Sciences*, vol. 27, no. 3, pp. 253–262, 2010.

[16] F. Tonicello and S. Vàzquez del Real, "Maximum point power tracker approach to a regulated bus," in *5th European Space Power Conference*, Tarragona, Spain, Sep. 1998, pp. 71–77.

[17] L. Croci, P. Della Putta, and A. Lazzeretti, "Maximum powerpoint tracker controller for unregulated bus architecture," in *7th European Space Power Conference*, Stresa, Italy, May 2005, pp. 1–6.

[18] M. R. Patel, *Spacecraft power systerm*. London: CRC Press Web, 2005.

[19] D. Sera, R. Teodorescu, and P. Rodriguez, "PV panel model based on datasheet values," in *IEEE International Symposium on Industrial Electronics*, Kuala Lumpur, Malaysia, Jun 2007, pp. 2392–2396.

[20] A. Chatterjee, A. Keyhani, and D. Kapoor, "Identification of photovoltaic source models," *IEEE Transactions on Energy conversion*, vol. 26, no. 3, pp. 883–889, 2011.

[21] H. Rahimi-Eichi, F. Baronti, and M. Y. Chow, "Modeling and online parameter identification of Li-Polymer battery cells for SOC estimation," in *IEEE International Symposium on Industrial Electronics*, Hangzhou, China, May 2012, pp. 1336–1341.

[22] A. Farmann and D. U. Sauer, "A study on the dependency of the open-circuit voltage on temperature and actual aging state of lithium-ion batteries," *Journal of Power Sources*, vol. 347, pp. 1–13, 2017.

[23] M. Ceraolo, "New dynamical models of lead-acid batteries," *IEEE Transactions on Power Systems*, vol. 15, no. 4, pp. 1184–1190, 2000.

[24] S. Asif and Y. Li, "Solar cell modeling and parameter optimization using simulated annealing," *Journal of Propulsion and Power*, vol. 24, no. 5, pp. 1018–1022, 2008.